IEEE Access
Multidisciplinary | Rapid Review | Open Access Journal

Received July 12, 2018, accepted September 14, 2018, date of publication October 25, 2018, date of current version November 30, 2018.

*Digital Object Identifier 10.1109/ACCESS.2018.2877956*

# Quasi-Distributed Fabry-Perot Optical Fibre Sensor for Temperature Measurements

**M. DELLA TAMIN AND JOHAN MEYER, (Senior Member, IEEE)**
School of Electrical and Electronic Engineering Science, University of Johannesburg at Auckland Park, Johannesburg 2006, South Africa
Corresponding author: M. Della Tamin (dellatamin@gmail.com)

**ABSTRACT** This paper presents a simulation and an experimental quasi-distributed Fabry–Perot optical fibre sensor for temperature measurements implemented on a serial array using a combined frequency division multiplexing and wavelength division multiplexing arrangement. Quasi-distributed fibre sensors have been of great interest in the industry for the monitoring of power transformers, jet engines, and furnaces. This paper is aimed at providing theoretical results for a quasi-distributed sensor system made of 25 local sensors imprinted on a serial array of the single mode fibre whereby the local sensors are of weak reflectivity. In addition, a sensor system of nine quasi-distributed local sensors is experimentally tested and a sensitivity of $10\frac{pm}{^{o}C}$ and a resolution of $0.125^{\circ}C$ are obtained. Its higher resolution, higher spatial distribution, and ability to measure temperature at different points simultaneously make it a very attractive temperature sensor.

**INDEX TERMS** Fabry-Perot, resolution, sensitivity, weak reflectivity.

## I. INTRODUCTION

Over the last few decades, optical fibre sensors (OFS) have been attractive in comparison to traditional electronic sensors because of numerous advantages which include light weight, electromagnetic immunity (EMI), and the ability to respond to a wide variety of physical parameters, small size, multiplex capability and remote sensing [1], [2]. OFSs are used for the monitoring of physical parameters such as pressure, strain, viscosity and temperature. Different types of OFSs have been successfully commercialized in the past few decades including Fabry-Perot fibre sensors, fibre optic gyroscopes and Fibre Bragg grating [3]. The Fibre Bragg grating (FBG) is a Bragg reflector which reflects particular wavelengths of light and transmits all others. A specific application of the FBGs is when they are used as mirrors to form an interferometer inside the fibre. In comparison to other optical fibre sensors, the Fabry-Perot interferometric fibre sensor presents many advantages associated with simplicity and compactness offering high resolution and sensitivity.

Fabry-Perot fibre sensors can be classified as extrinsic or intrinsic. Extrinsic Fabry-Perot interferometric (EFPI) fibre sensors typically result from two fibers physically separated by an air gap but connected by a capillary. EFPI fabrication is relatively simple, but suffers from problems such as alignment, low coupling efficiency and packaging [4]. In the Intrinsic Fabry-Perot Interferometric (IFPI) sensor configuration, the sensing element is the fibre itself. The mirrors that form the cavity are merged to the fibre by micromachining [5], [6], UV irradiation [7], [8], chemical etching [9], or thin film deposition [10], [11]. FBG based Fabry-Perot fibre sensors have been developed and experimentally tested as point sensors for strain monitoring [12], for temperature monitoring [13], and as quasi-distributed sensors for reinforced concrete monitoring [14], for precast concrete monitoring [15] and for temperature monitoring [16]. Different interrogation schemes for Fabry-Perot based FBG fibre sensors have been investigated and implemented including optical time domain reflectometry (OTDR), white light interferometry and Fourier transform (FT). Interrogating a local cavity Fabry-Perot fibre sensor with white light interferometry using the wavelength tracking method, the sensor's resolution is higher [17]. In the multiplexed situation, the wavelength tracking is a challenge due to the superimposition of the spectrum [18]. In such a case, the Fourier transform method is preferred since each respective local sensor can be directly interrogated.

In this paper, we present a theoretical simulation of a quasi-distributed FBG based Fabry-Perot sensor system in a configuration of 25 local sensors. To better highlight the simulations, an experimental sensor system consisting of 9 FBG based Fabry-Perot local sensors is designed, tested and presented. In both cases, the FT algorithm is used to measure temperature changes in the interrogated sensors.

## II. THEORETICAL CONCEPTS

The FBG based Fabry-Perot sensor is composed of two identical gratings of weak reflectivity separated by a cavity. The gratings are therefore identical in their respective wavelength

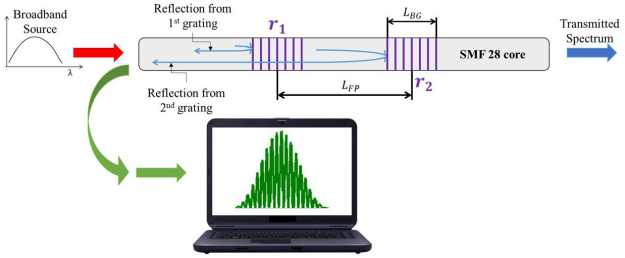


**FIGURE 1.** Weak-reflectivity identical local cavity.

and reflectivity. A typical setup of a FBG based Fabry-Perot local cavity is presented in Fig. 1. When a broadband light spectrum source is coupled into the optical fibre as shown in Fig. 1, as it propagates down the fibre, a selective wavelength of weak-reflectivity is reflected by the first and second gratings. As the remaining light spectrum propagates down the fibre, the reflected spectrum propagating towards the optical source produce an interference pattern captured on the detection system. The spectrum captured on the detection system is defined as [13],

$$R(\lambda) = 2\left[\frac{\pi n_{eff} L_{BG}}{\lambda} \text{sinc} \frac{2n(\lambda - \lambda_{BG})}{\lambda\lambda_{BG}}\right]^2 \times \left(1 + \cos\left(\frac{4\pi n L_{F-P}}{\lambda}\right)\right), \quad (1)$$

where: $\lambda_{BG}$ is the Bragg wavelength, $\lambda$ is the wavelength from the source, $n_{eff}$ is the effective refractive index and $n$ is the mean refractive index of the fibre.

The spectrum represented by (1) is composed of two parts namely the spectrum of the Bragg grating represented by $2\left[\frac{\pi n_{eff} L_{BG}}{\lambda} \text{sinc} \frac{2n(\lambda-\lambda_{BG})}{\lambda\lambda_{BG}}\right]^2$ known as the envelop function and the interference pattern represented by $\left(1 + \cos\left(\frac{4\pi n L_{F-P}}{\lambda}\right)\right)$. The frequency of the reflected interference pattern is greatly dependent on the separation between the two identical gratings as defined by [16] and presented in (2).

$$f = \frac{2nL_{F-P}}{\lambda_{BG}^2}, \quad (2)$$

where: $n$ is the refractive index inside the cavity, $L_{F-P}$ is the cavity length and $\lambda_{BG}$ is the Bragg wavelength of the mirrors.

In a simulation situation, the cavity length ($L_{F-P}$) shown in (2) can be manipulated to see its impact on the frequency of the interference pattern. This is aimed at finding the cavity size whereby the interference pattern is still captured on the detection system. In a quasi-distributed configuration, the local sensors are implemented on a serial array in a frequency division multiplexing (FDM) or wavelength division multiplexing (WDM). A typical quasi-distributed FBG based Fabry-Perot sensor system is presented in Fig. 2. In a FDM configuration, all the Fabry-Perot local sensors are of weak-reflectivity and identical wavelength then separated

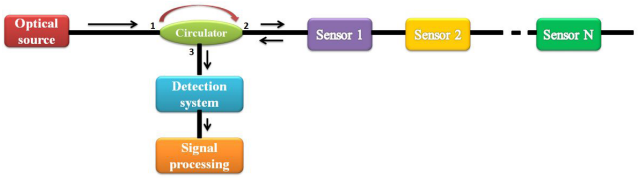


**FIGURE 2.** Quasi-distributed Fabry-Perot fibre sensor theoretical setup.

from one to the other at an appropriately designed distance in such way to avoid cross talks. The use of weak reflectivity gratings reduces the optical power loss at each local sensor to the minimum [8], [19]. In this configuration, the local sensors differ from one to the other in their respective cavity length. Having cavities of different length warrant interference pattern at different frequencies. In such way, all the reflected interference pattern from all the local sensors in the sensor system superimposed themselves to form the total reflected spectrum observed on the detection system. This total reflected interference pattern is centered to the wavelength of the identical gratings represented by:

$$R_T(\lambda) = \sum_{j=1}^{N=5} R_j(\lambda), \quad (3)$$

where $N$ represents the number of interference patterns produced from N weak-reflectivity identical local sensors. In a WDM configuration, the identical gratings that form the cavity are of weak-reflectivity. The FBG that form the cavity differ from one cavity to the other, as well as their respective cavity length. When the broadband light source is coupled into the fibre, each respective local sensor reflects an interference pattern. Each interference pattern is centered at respective cavity grating's wavelength. The total reflected spectrum is also theoretically described by (3). In a combined configuration of FDM and WDM, the optical system is aimed at increasing the multiplexing capability of the system. In such arrangement, number of local sensors are implemented in a frequency multiplexed setup whereby all the gratings are of identical wavelength and weak-reflectivity. Having different wavelength channels as described in WDM, considerable amount of local sensor can be realized on the sensor system. The total reflected spectrum is the combination of the superimposed reflected spectrums from the local sensors having identical wavelength per wavelength channel.

## III. SENSORS SIMULATION

The reflectivity of the FBG representing the mirrors in the Fabry-Perot configuration are designed and simulated using the well-known coupled mode theory before they are used as reflective mirrors in the Fabry-Perot cavity. These FBGs are theoretically implemented using the parameters of the single mode fibre (SMF 28) - such as the refractive index, thermal expansion and thermo-optic effect coefficients. A white noise having a Gaussian profile of $\sigma = 0.1$ known as standard deviation is added to the phase of (1) and sampled with a resolution of 5 pm, then simulated thereafter using Matlab

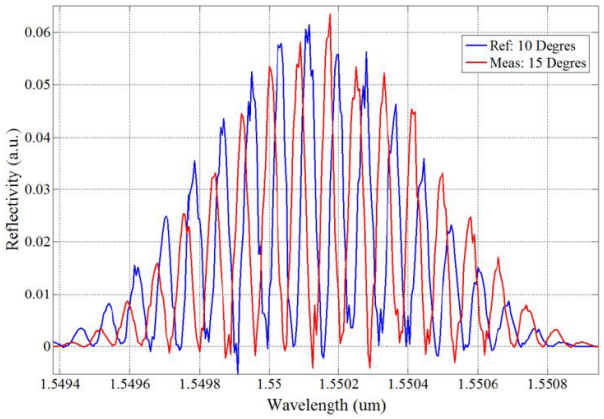


**FIGURE 3.** Local sensor spectrum.

as a tool. The simulated local sensor is presented in Fig. 3. The spectra presented in Fig. 3 are the responses of the local sensor 1 calibrated at $10°C$ and the instantaneous variation at $15°C$. Clearly as stated by Miridonov *et al.* [13], the noise does not affect the shape of the interference pattern as it can be seen by the ripples on the spectrums, but affects its phase. In the FDM configuration, 5 local sensors are implemented whereby all the gratings forming the cavities are identical in wavelength (1550 nm) and in reflectivity. The local sensors are 30 cm from each other and their cavity length ranging from 1 cm to 5 cm with an increment of 1 cm respectively. As light from the broadband source is coupled into the sensor system, a low percentage of its spectrum is reflected by the first and second gratings. The setup of this configuration is presented in Fig. 2. In its working, the transmitted spectrum from the first local sensor becomes the incident wave of the second local sensor and the above phenomena occur again. The above phenomenon is repeated until the last sensor of the system. Having added a white noise with a Gaussian profile to the phase of (3), the total reflected spectrum captured on the detection system is presented in Fig. 4.

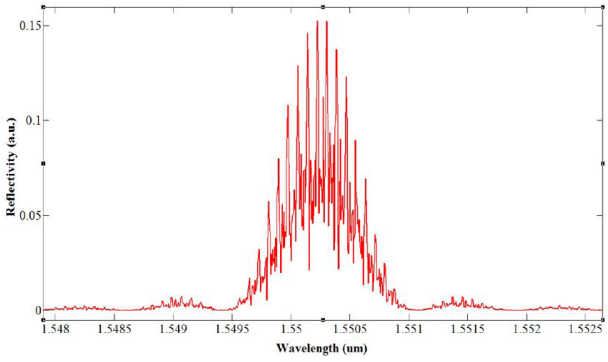


**FIGURE 4.** Quasi-distributed FDM fibre sensor system total reflected spectrum.

The total spectrum reflection is the superimposition of all interference patterns generated by all local sensors as shown in Fig. 4. The WDM configuration is made of 5 wavelength

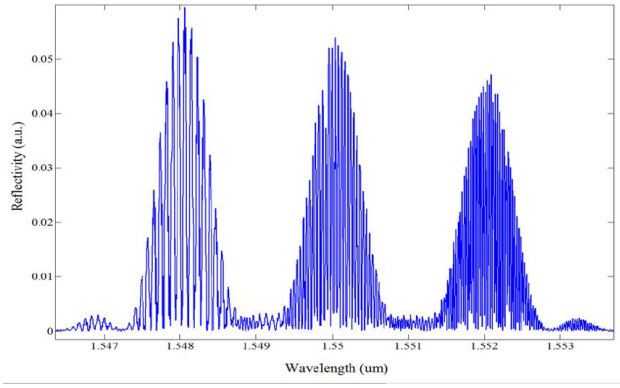


**FIGURE 5.** Quasi-distributed WDM fibre sensor system total reflected spectrum.

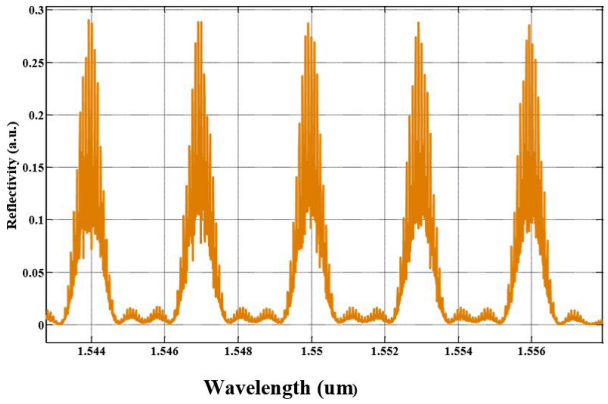


**FIGURE 6.** Combined FDM and WDM sensor system total reflected spectrum.

channels having a single local sensor in each wavelength. The designed cavity lengths ranges from 1 cm to 5 cm having an increment of 1 cm. Based on the setup in Fig. 2, their respective wavelength is designed to 1546 nm, 1548 nm, 1550 nm, 1552 nm and 1554 nm respectively and its total reflected spectrum presented in Fig. 5. As it can be observed from Fig. 5, each local sensor has a specific interference pattern frequency that is defined by the cavity length respectively. Each interference pattern is centered to the wavelength of the gratings that form the individual cavity. By conceptualizing the sensor system described in WDM of 5 channels and in FDM made of 5 local sensors, 25 local sensors are designed on the serial array of the SMF 28. Under proper working conditions, the total reflected spectrum is presented in Fig. 6. It can be observed from Fig. 6 that the interference pattern superimposes themselves per wavelength channel. All the superimposed spectrum per wavelength channels are of almost equal reflectivity. This is since all the gratings are of identical weak-reflectivity.

## IV. DEMODULATION THEORY

This section presents the algorithm used to evaluate temperature changes in each respective local sensor. Changes in temperature in each respective local sensor causes a shift of

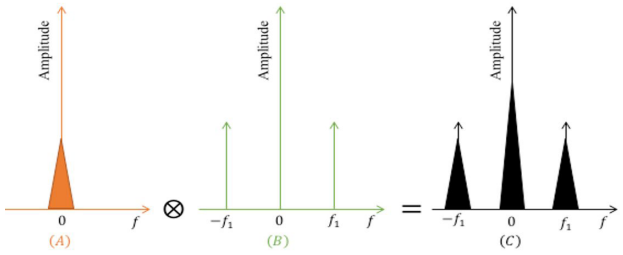


**FIGURE 7.** Triangle shapes transformation.

its reflected interference pattern in the wavelength domain. The demodulation algorithm used in this paper to evaluate temperature changes is based on Fourier Transform (FT) shift analysis. When temperature changes, so does the reflected interference pattern in the wavelength domain. This variation of temperature induces changes in phase in Fourier domain. By evaluating changes in phase, temperature changes can be measured. By applying Fast Fourier Transform (FFT) to the captured reflected spectrum in wavelength domain, the resulting spectrum is presented in the form of triangle shapes [13]. The triangle shapes presented in Fig. 7 result from the convolution of the envelop function and the interference pattern described in Equation 1. From the explanations of the plots on Fig. 7, the FT of a constant is known as a $\delta$-function centered at the origin. The FT of a cosine function produces two $\delta$-functions, one centered at the frequency of the cosine function and the other mirrored to the left side of the origin as shown. Furthermore, the FT of the Bragg grating represented by $2\left[\frac{\pi n_{eff} L_{BG}}{\lambda}\text{sinc}\frac{2n(\lambda-\lambda_{BG})}{\lambda\lambda_{BG}}\right]^2$ yields a triangle function. Therefore, the convolution in Fourier domain of the grating and the cosine function generates the triangle shapes presented in Fig. 7 (C). On the plot of the triangle shapes represented by Fig. 7 (C), the signal amplitude of the component at 0 frequency of the local sensor's reflected spectrum in Fourier domain is known as the offset, and the triangle shape at the left (-$f$1) is a mirror image of the one at the right ($f$1), which is the signal of the sensor. The triangle shapes are characterized by their spectral width which are a function of the Bragg wavelength and the refractive index of the fibre in Fourier domain, as presented [20].

$$\Delta f_{BG} = \frac{4nL_{BG}}{\lambda_{BG}^2}. \tag{4}$$

Since the FT is made up of samples, so are the triangles shapes constituted with few samples having a band-width as defined by Equation 4. This band-width limited in both sides by a minimum and a maximum frequency represented as:

$$f_{max/min} = f \pm \frac{\Delta f_{BG}}{2} = \frac{2n(L_{F-P} \pm L_{BG})}{\lambda_{BG}^2}, \tag{5}$$

where: $f$ is the frequency of the interference pattern of the local sensor, $\Delta f_{BG}$ is the spectral bandwidth, $f_{max}$ is the local sensor maximum frequency and $f_{min}$ is the local sensor minimum frequency in the triangle shape. In order to recover the information kept inside the respective local sensor, the Nyquist theorem is applied to sample the signal in Fourier domain [13]. Such inclusion of the Nyquist theorem yields the sampling frequency as:

$$f_m \geq \frac{2 \times 2n(L_{BG} + L_{F-P})}{\lambda_{BG}^2}, \tag{6}$$

where: $f_m is$ the sampling frequency. When the system is calibrated, the captured spectrum presented in (1) is now represented by $R_{F-P}(f)$ where no disturbance has been applied to the sensor. When disturbance is applied, the captured spectrum is now represented by $R'_{F-P}(f)$. The evaluation of temperature changes is done by evaluating the relative phase shift between the calibrated reference spectrum and the instantaneous measured spectrum. In the case of no disturbance, the relative phase difference is zero. The calculation of the relative phase is presented as:

$$\phi_m = \arg[R'_{F-P}(f) \times R^*_{F-P}(f)], \tag{7}$$

where $R^*_{F-P}(f)$ is the complex conjugate of the calibrated spectrum of the local sensor and $\phi_m$ is the relative phase as function of samples in Fourier domain. Interferometric fibre sensors experience a $2\pi$ problem that need to be addressed after calculation of the relative phase. Interferometric fibre sensors give the same values for phases, which differ by multiples of $2\pi$ and are known as the ambiguity caused by the cosine function presented in Equation 1 [13]. The ambiguity can be addressed using linear regression. Knowing the relative phase and the ambiguity gives the possibility to evaluate the total phase shift induced temperature changes.

$$\phi_{Abs} = \phi_{relative} + 2\pi M. \tag{8}$$

In the quasi-distributed sensor system, the total reflected spectrum captured on the detection system is Fourier transformed. The FT spectrum is presented in the form of multiple triangle shapes where each triangle shape located at the right-hand side of the frequency zero represents the respective local sensors information. Each local sensor is centered on its respective interference pattern frequency, represented by [13]:

$$f_j = \frac{2nL_{(F-P)_j}}{\lambda_{BGj}^2}, \tag{9}$$

where $f_j$ represents the frequency of the $j^{th}$ local sensor, $\lambda^2_{BG_j}$ represents the Bragg wavelength of the $j^{th}$ local sensor and $L_{(F-P)_j}$ represents the cavity length of the $j^{th}$ local sensor. The frequency band-width of each respective local sensor is represented as:

$$\Delta f_{BGj} = \frac{4nL_{BGj}}{\lambda_{BGj}^2}, \tag{10}$$

where $L_{BG_j}$ represents the Bragg grating length of the $j^{th}$ local sensor. In a fibre Bragg grating-based F-P multiplexed configuration implemented in series, cross-talk originates from reflectance of any of the two mirrors which influence the

**TABLE 1. Quasi-distributed sensor system characteristics.**

| Designation | Formulas |
|---|---|
| Minimum cavity length | $L_{(F-P)min_j} \geq 2L_{BG_j}$ |
| Maximum cavity length | $L_{(F-P)max_j} \leq \frac{\lambda_{BG}^2}{4nF}$ |
| Minimum difference between local sensors | $L_{(F-P)_j} - L_{(F-P)_{j-1}} \geq 2L_{BG}$ |
| Separation between local cavities | $L_{minimum\_length} > \frac{\lambda_{BG}^2}{4nF}$ |

readings of the sensor's array. The analysis of the cross-talks in this sensor system yields an important task in lowering their effects in the demodulation is based on description provided by [21]. Using the SLED as optical source, and weak reflectivity gratings as reflectors in the local sensors, minimize the impact of the cross-talks as well. This is due to the low attenuation of the SMF in the 1550 nm region and the low losses related to the low-reflectivity of the identical-gratings and then to the low coherence length of the broadband source. Therefore, the cross-talks is negligible and their effects on the sensor system are limited.

## V. CHARACTERISTICS OF THE SENSOR SYSTEM

This section is aimed at describing restrictions on the minimum and maximum cavity length, the separation between consecutive local sensors and the difference in length between 2 consecutive local cavities. The minimum length of the F-P cavity is the limitation on the separation between the two identical gratings, wherein the interference pattern of local sensor can still be recovered for proper demodulation. The spectral width of the grating and the frequency of the interference of the local sensor are very important parameters used to size the minimum cavity length. On the other hand, the maximum cavity length of the local sensor is the acceptable length whereby the interference pattern fringes can still be resolved by the detection system for proper demodulation. This is because the separation of the fringes in F-P interferometer is a function of the cavity length. The minimum separation of the fringes depends on the resolution of the detection system. Therefore, if the resolution of the detection system is not enough to separate the fringes, information is lost. The separation between local sensors should be carefully designed to avoid confusion in the demodulation. In the quasi-distributed sensor systems, the rule of thumb says that the minimum separation between 2 local sensors should be bigger than the largest cavity length on the system. The minimum difference in length between local sensors had to be established to prevent an overlap when the Fourier analysis is performed. From the theory, these characteristics have been defined by[13], [16], and [20] as presented in Table 1. When the F-P sensor system is implemented in series, cross-talk originates from reflectance of any of the two mirrors which influence the readings of the sensor's array. The analysis of the cross-talks in this sensor system yields an important task in lowering their effects in the demodulation. Since any two mirrors interact with the incident light, the reflectance and the transmittance of the $j^{th}$ local sensor are respectively represented by $R_j$ and $T_j$. The transmittance of the $j^{th}$ local sensor is as described by Shen, 2006. Shen further describes mathematically the normalization of the cross-talks showing their low impact on the performance of the sensors using the SMF 28 [21]. A continuous wave (CW) COVEGA Thor-Labs model SLD1005S super luminescent emitting diode (SLED) was used during the measurements as optical source with center wavelength $\lambda_C = 1549\,nm$, 49.6 nm optical bandwidth and $P_{ASE} = 27.6\,mW$. Its working principles are based on super-luminescence [22]. Its coherence length is shorter as compared to that of a diode laser. Using weak reflectivity gratings as reflectors in the local sensors, minimized the impact of the cross-talks as well. Therefore, cross-talk amplitude was negligible and their effects on the sensor system limited.

## VI. SENSOR MONITORING

The monitoring of the sensor systems presented in this paper is based on the demodulation theory explained in Section 4. This demodulation theory provided a strong background in the monitoring of temperature changes in the respective local sensors. In each respective local sensor, changes in temperature generate changes in respective reflected interference pattern in wavelength domain. The respective changes in wavelength domain produce changes in the phase of the interference pattern when FT is applied as explained. By evaluating changes in phase, changes in temperature can be measured. Having 25 local sensors along the single array of the optical fibre allows quasi-distributed temperature sensing. Five gratings wavelengths were selected for the 25 sensors system namely 1544 nm (channel A), 1546 nm (Channel B), 1550 nm (channel C), 1552 nm (channel D) and 1554 nm (channel E). Cavities of 1 cm, 2 cm, 3 cm, 4 cm and 5 cm were chosen per channel respectively as local sensor 1, 2 up to 5. This set up was intended to achieve a combined FDM and WDM multiplexing on the single length of the SM28 fibre where each Bragg wavelength represented a channel of five local sensors designed in FDM setup. Due to the robustness of the demodulation, each reflected spectrum per channel can be retrieved and interrogated. This interrogation should enable to access each respective local sensor in respective wavelength channels. Applying the FT to the wavelength channel A, referring to 1544 nm, The Fourier domain spectrum of the 5 local sensors implemented in a FDM is presented in Fig. 8. After applying the FT to the respective window around the 1544 nm spectrum in the wavelength domain, it yields 5 triangle shapes representing the respective local sensors in channel A. The triangle centered at frequency = 0, has information from the 5-weak reflectivity identical-gratings forming the local sensors in that respective wavelength channel. Other triangles shapes are centered to the frequency of their respective interference patterns. As it can be observed, all triangles shapes have same broad-width,

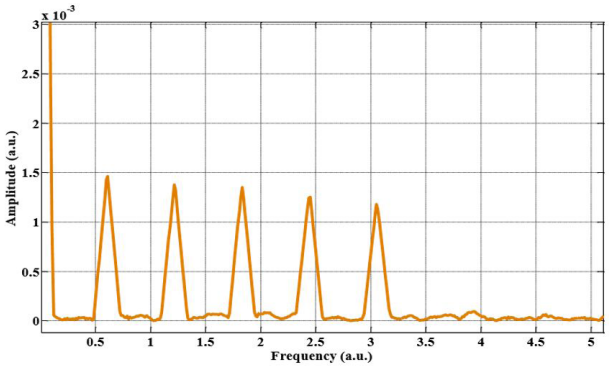


**FIGURE 8.** Fourier transform of 5 local sensors in the wavelength channel A.

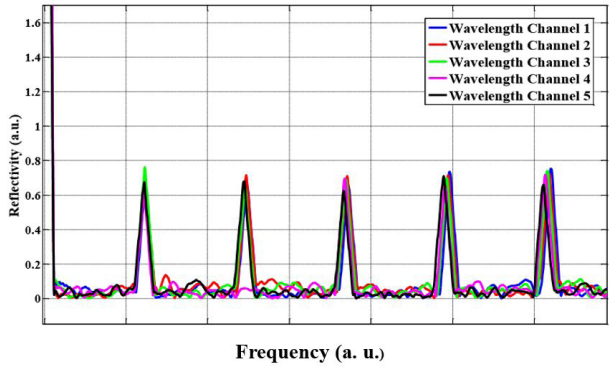


**FIGURE 9.** FT of 15 local sensors plotted on a single figure.

which depends on the characteristics of the Bragg gratings. Hence, having 25 weak-reflectivity identical grating local sensors, the Fourier transform spectrum is a set of 25 triangle shapes. The shift of each weak-reflectivity identical-gratings local sensor interference pattern in Fourier domain is be detected as the phase shift in the corresponding local sensor as described by [13]. On the sensor system of 25 local sensors, all the triangle shapes are plotted on the single plot presented in Fig. 9. Fig. 9 is a broadened FT spectrum of the entire sensor system's reflected spectrum in wavelength domain. Each wavelength channel is presented by a specific color as shown. Using the demodulation algorithm presented by Miridonov *et al.* [13], each local sensor can be individually interrogated per wavelength channel as explained. Therefore, phase response to temperature changes can be measured.

## VII. EXPERIMENTAL SETUP

The optical setup is made of 9 local sensors in this experiment. All the local sensors are imprinted on a single array of the single mode fibre using an Argon laser as presented in Fig. 10. The designed quasi-distributed sensor system is arranged in 3 distinct WDM channels, that is, 1550 nm, 1555 nm and 1560 nm respectively. Each wavelength channel consists of 3 local sensors configured in a FDM, whereby the $1^{st}$, $2^{nd}$ and $3^{rd}$ local sensor have a 1 cm, 2 cm and

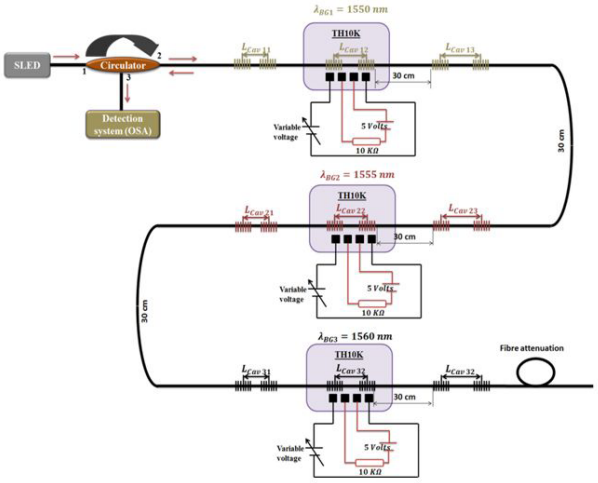


**FIGURE 10.** Experimental setup made of 9 local sensors.

3 cm cavity length respectively as presented on Fig. 10. In this temperature monitoring experiment, the 2nd local sensor of each wavelength channel is affected by temperature changes, while the others are not. Each of the affected local sensors is placed on a thermal plate inside distinct plastic glass boxes. The used of the thermal plate is aimed at providing temperature changes on the fibre sensors. The change in temperature is controlled using two power supplies for each interrogated local sensor. The purpose of this experiment is to show the results of the 3 local sensors in different channels. All the printed local sensors are of weak-reflectivity (0.2%) and are identical in wavelength per channel. Due to having such weak-reflectivity mirrors, many local sensors can be printed on the same serial array of the SMF fibre and furthermore, the effect of cross talks is considerably minimized. The local sensors are 30 cm apart from each other and are all printed on a 4 m fibre. During temperature monitoring, 3 distinct power supplies (PS) are used to power the thermal plates and the other 3 PS are used to control the temperature at different thermistors. Before the calibration of the system for temperature measurements, the total reflected spectrum of the optical system is presented in Fig. 11. As presented in Fig. 11, the respective amplitude of the sub-total interference pattern of the 3 wavelength channels is almost identical, which is as expected by design. However, the slight difference in height of the interference pattern of the respective wavelengths, illustrated in Fig. 11, can be attributed to the printing process. This process has not been automated, so it can be assigned to the human factor during the imprint process. After the calibration, temperature is induced on the thermal plate by incrementing the voltage from the power supply of 0.1 V every 5 minutes corresponding approximately to $2°C$. Fourier transform algorithm presented by [13] is applied to the captured spectrum and each respective local sensor is interrogated individually. Quasi-distributed sensor system response to temperature changes is a combination of all the interrogated local fibre

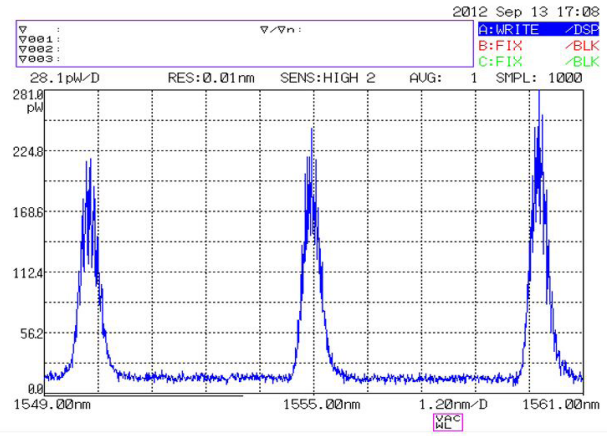


**FIGURE 11.** Total reflected spectrum of the experimental measurement.

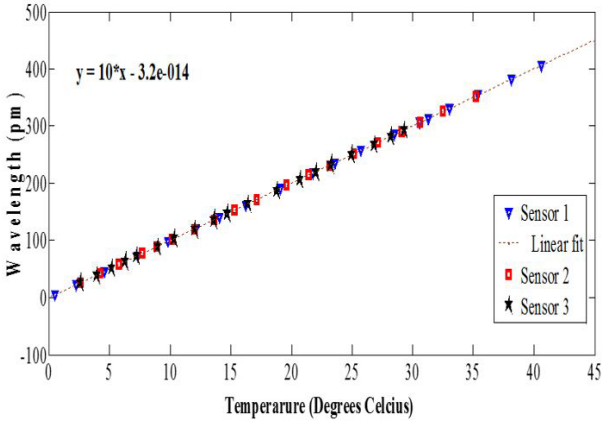


**FIGURE 12.** Experimental response of 9 local sensors to temperature changes.

sensors presented on the same plot in Fig. 12. As shown in Fig. 12, the graph in blue represents the local fibre sensor affected in wavelength channel 1, while the graphs in red and black represent the local sensors affected in wavelength channel 2 and wavelength channel 3 respectively. Their respective responses to temperature changes overlap regardless of their wavelength channels. This is because all the affected local fibre sensors that have similar cavity lengths have been optimally imprinted. These results agree with the literature. The difference in temperature from different local sensors is due to their respective thermal plates' characteristics. In this experiment, the performance of the sensor system is tested. In this regard, a temperature sensitivity of $10\frac{pm}{^oC}$ and a temperature resolution of 0.125 are achieved showing the enormous potentials in this interferometric sensor type. The lab experimental setup is presented on Fig. 13. The local sensors have been placed inside the plastic boxes on the thermal plates used as resistive foil heaters having a 10 $k\Omega$ thermistor directly integrated into the plates and 4 terminals. Each thermistor is a negative temperature coefficient (NTC) thermistor which the resistance decreases when the temperature increases. The OSA screen to capture the interference

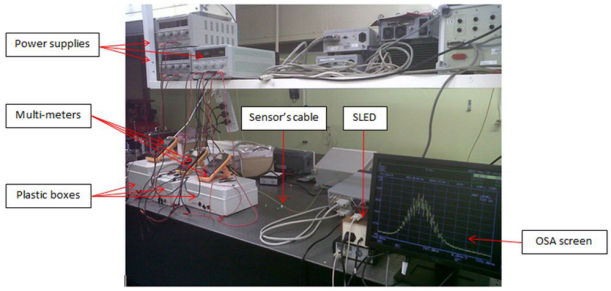


**FIGURE 13.** Lab experimental setup for the 9 local sensors monitoring of temperature changes.

patterns, power supply to power the thermal plates, the SLED to provide optic power and the multi-meters are also displayed on Fig. 13.

## VIII. DISCUSSIONS

The theory of the fibre Bragg grating-based F-P interferometer used in this article is not new. It has been developed and used in various applications to monitor multiple physical parameters. The Fourier Transform demodulation algorithm has been developed for temperature and strain in multiplexing configurations [13], [16], [20]. It is understood that the algorithm of the Fourier transform demodulation algorithm incorporates and takes into account the Nyquist-Shannon theories and the restrictions over cavity lengths. Cross-talks have been presented in this article to quantify its impact on the operation of the sensor system. Its impact was found minimal in this sensor system using a broadband source and a single mode fibre. The sensor system presented in this paper could be optimized for applications in dense sensing environments. In such a situation and based on the broad-width of the triangular shapes on the FFT spectrum, 4 additional triangular shapes representing extra local sensors could be inserted on the FFT spectrum with neither overlap and nor loss of information during the demodulation. As a rule of thumb, this would result in 20 cm separation between the local sensors. The new sensor system configuration could accommodate 45 local sensors. This number can be further optimized to more sensors on the array depending on the application. Such a dense configuration has been developed, simulated [19] and then configured with 9 local sensors in a FDM/WDM layout [23]. This system could be optimized up to 1000 local sensors. From the 9 local sensors developed and presented, a sensor resolution of $0.4°C$ has been accomplished [23].

Compared to the resulted of $0.4°C$, the sensor system presented in this paper achieved a resolution of $0.125°C$ and a temperature sensitivity of $10\frac{pm}{^oC}$. This resolution was obtained after a long set of measurements in each interrogated local sensor of 50 data recorded every 15 minutes. The processed phase shift data was plotted, and its standard deviation was evaluated and then used to calculate the average resolution of the sensor. The sensitivity obtained in this sensor was as

expected in the literature while its resolution can be considered important. The reason of this might be attributed to the robustness of the demodulation algorithm, and to the quality of the instruments used.

## IX. CONCLUSION

An overview on the intrinsic interferometric Fabry-Perot quasi-distributed fibre sensor for temperature measurements was presented. We first have provided a brief explanation on the FBG based Fabry-Perot fibre sensor and its working principle. A simulation of a combination of 25 local sensors in a system whereby each first local sensor in the wavelength channels having 1 cm cavity length was interrogated. This has opened the doors to a better understanding of the system in order to design and build an optical setup of a quasi-distributed sensor system of 9 local sensors imprinted on the single array. The demodulation algorithm (Fourier Transform) described by [13] was identically applied to both simulation and experiment and the results obtained from the simulations have led to the development of the experimental testing of the quasi-distributed sensor. Their respective results overlapped. The repeatability of the results obtained from the experimented sensor system and their hysteresis has been assessed and is in conformity with the expectations. The cross-talks as derived and presented by [21] have been also discussed to understand their impact on the functioning of the sensor system discussed. Therefore, based on the performance of the 9 tested and interrogated local sensors, the respective results of 10 $\frac{pm}{^oC}$ temperature sensitivity and $0.125°C$ resolution have been achieved. This sensor clearly shows potentials in dense multiplexing.

## REFERENCES

[1] B. Culshaw, "Fiber-optic sensors: Applications and advances," *Opt. Photon. News*, vol. 16, no. 11, pp. 24–29, 2005.
[2] E. Udd, R. J. Michal, S. F. Watanabe, J. P. Theriault, and R. F. Cahill, "Fiber optic sensors," U.S. Patent 4 787 741, Nov. 29, 1988.
[3] Q. Wang *et al.*, "Study on characteristics of EFPI pressure sensors for HT/HP oilwell," *Optoelectron. Adv. Mater.-Rapid Commun.*, vol. 5, no. 9, pp. 1021–1025, 2011.
[4] J. S. Sirkis, D. D. Brennan, M. A. Putman, T. A. Berkoff, A. D. Kersey, and E. J. Friebele, "In-line fiber étalon for strain measurement," *Opt. Lett.*, vol. 18, no. 22, pp. 1973–1975, 1993.
[5] T. Wei, Y. Han, H.-L. Tsai, and H. Xiao, "Miniaturized fiber inline Fabry–Perot interferometer fabricated with a femtosecond laser," *Opt. Lett.*, vol. 33, no. 6, pp. 536–538, 2008.
[6] Z. Ran, Y. Rao, J. Zhang, Z. Liu, and B. Xu, "A miniature fiber-optic refractive-index sensor based on laser-machined Fabry–Perot interferometer tip," *J. Lightw. Technol.*, vol. 27, no. 23, pp. 5426–5429, Dec. 1, 2009.
[7] X. Wan and H. F. Taylor, "Intrinsic fiber Fabry–Perot temperature sensor with fiber Bragg grating mirrors," *Opt. Lett.*, vol. 27, no. 16, pp. 1388–1390, 2002.
[8] Z. Wang, F. Shen, L. Song, X. Wang, and A. Wang, "Multiplexed fiber Fabry–Pérot interferometer sensors based on ultrashort Bragg gratings," *IEEE Photon. Technol. Lett.*, vol. 19, no. 8, pp. 622–624, Apr. 15, 2007.
[9] V. R. Machavaram, R. A. Badcock, and G. F. Fernando, "Fabrication of intrinsic fibre Fabry–Perot sensors in silica fibres using hydrofluoric acid etching," *Sens. Actuators A, Phys.*, vol. 138, no. 1, pp. 248–260, Jul. 2007.
[10] P. Morris, A. Hurrell, A. Shaw, E. Zhang, and P. Beard, "A Fabry–Pérot fiber-optic ultrasonic hydrophone for the simultaneous measurement of temperature and acoustic pressure," *J. Acoust. Soc. Amer.*, vol. 125, no. 6, pp. 3611–3622, 2009.
[11] J.-R. Zhao, X.-G. Huang, W.-X. He, and J.-H. Chen, "High-resolution and temperature-insensitive fiber optic refractive index sensor based on Fresnel reflection modulated by Fabry–Perot interference," *J. Lightw. Technol.*, vol. 28, no. 19, pp. 2799–2803, Oct. 1, 2010.
[12] B. Yan, P. A. Childs, C. Yu, X. Sang, D. Xu, and G.-D. Peng, "Spectrally coded multiplexing based on FBG pairs," in *Session 3P4b Microwave Devices, Propagation*. Cambridge, MA, USA: PIERS, 2010, p. 543.
[13] S. V. Miridonov, M. G. Shlyagin, and D. Tentori, "Twin-grating fiber optic sensor demodulation," *Opt. Commun.*, vol. 191, nos. 3–6, pp. 253–262, 2001.
[14] S. Tjin, Y. Wang, X. Sun, P. Moyo, and J. M. W. Brownjohn, "Application of quasi-distributed fibre Bragg grating sensors in reinforced concrete structures," *Meas. Sci. Technol.*, vol. 13, no. 4, p. 583, 2002.
[15] L. Rodriguez-Cobo, J. A. Polanco, A. Quintela, I. A. Carrascal, and J. M. López-Higuera, "Quasidistributed fiber sensor for precast concrete structures monitoring," *Proc. SPIE*, vol. 8421, p. 84214R, Oct. 2012.
[16] M. G. Shlyagin, S. V. Miridonov, I. M. Borbon, V. V. Spirin, P. L. Swart, and A. A. Chtcherbakov, "Multiplexed twin Bragg grating interferometric sensor," in *15th Opt. Fiber Sensors Conf. Tech. Dig.*, May 2002, pp. 191–194.
[17] V. Bhatia, M. B. Sen, K. A. Murphy, and R. O. Claus, "Wavelength-tracked white light interferometry for highly sensitive strain and temperature measurements," *Electron. Lett.*, vol. 32, no. 3, pp. 247–249, Feb. 1996.
[18] W. Wang, D. Ding, N. Chen, F. Pang, and T. Wang, "Quasi-distributed IFPI sensing system demultiplexed with FFT-based wavelength tracking method," *IEEE Sensors J.*, vol. 12, no. 9, pp. 2875–2880, Sep. 2012.
[19] J. T. G. Bonilla, A. G. Bonilla, V. M. R. Betancourtt, H. G. Bonilla, and A. C. Zamora, "A theoretical study and numerical simulation of a quasi-distributed sensor based on the low-finesse Fabry–Perot interferometer: Frequency-division multiplexing," *Sensors*, vol. 17, no. 4, p. 859, 2017.
[20] M. G. Shlyagin, S. V. Miridonov, D. Tentori, and J. Castillo, "Twin grating-based interferometric fiber sensor," in *Proc. Opt. Fiber Sensors*. Washington, DC, USA: OSA, 1997, p. OThC17.
[21] F. Shen, "UV-induced intrinsic Fabry–Perot interferometric fiber sensors and their multiplexing for quasi-distributed temperature and strain sensing," Ph.D. dissertation, Center Photon. Technol., Bradley Dept. Elect. Comput. Eng., Virginia Tech, Blacksburg, VA, USA, 2006.
[22] R. Paschotta, *Encyclopedia of Laser Physics and Technology*, vol. 1. Berlin, Germany: Wiley, 2008.
[23] X. Li *et al.*, "Simultaneous wavelength and frequency encoded microstructure based quasi-distributed temperature sensor," *Opt. Express*, vol. 20, no. 11, pp. 12076–12084, 2012.

**M. DELLA TAMIN** was born in Nkongsamba, Littoral, Cameroon, in 1970. He received the B.S. degree in electrical and electronic engineering and the M.S. degree in photonics from the University of Johannesburg, South Africa, in 2010 and 2014, respectively, where he is currently pursuing the Ph.D. degree in engineering management.

He was the Head of the Department for P2 Projects, an internship program rolled out by Resolution Circle to facilitate the graduation of engineering diplomates in South Africa. Since 2013, he has been an Electrical Engineer with Resolution Circle that is the University of Johannesburg owned company, where he is currently with the Professional Training Department.

**JOHAN MEYER** was born in Johannesburg, South Africa, in 1966. He received the Dipl.Ing. degree in electrical engineering from Rand Afrikaans University in 1992. He was the Head of the Photonics Research Group, where he was appointed as the Head of the School for Electrical Engineering. He worked for aeronautical industry for 12 years and joined the University of Johannesburg in 2004, where he is currently an Associate Professor with the Faculty of Engineering and the Built Environment. He is currently a registered Professional Engineer. His fields of expertise include fiber optical sensors and systems engineering.